File Copy

AD [illegible]

BRL R 1454

BRL

REPORT NO. 1454

QUALITATIVE INTERFEROMETRY OF EXPANDING METAL VAPOR

by

F. D. Bennett
G. D. Kahl
F. N. Weber, Jr.

October 1969

U.S. ARMY ABERDEEN RESEARCH AND DEVELOPMENT CENTER
BALLISTIC RESEARCH LABORATORIES
ABERDEEN PROVING GROUND, MARYLAND

B A L L I S T I C   R E S E A R C H   L A B O R A T O R I E S

REPORT NO. 1454

OCTOBER 1969

QUALITATIVE INTERFEROMETRY OF EXPANDING METAL VAPOR

F. D. Bennett
G. D. Kahl
F. N. Weber, Jr.

Exterior Ballistics Laboratory

RDT&E Project No. 1T061102A33D

A B E R D E E N   P R O V I N G   G R O U N D,   M A R Y L A N D

BALLISTIC RESEARCH LABORATORIES

REPORT NO. 1454

FDBennett/GDKahl/FNWeber/smo
Aberdeen Proving Ground, Md.
October 1969

QUALITATIVE INTERFEROMETRY OF EXPANDING METAL VAPOR

ABSTRACT

The metal vapor from a wire exploded in a gas is assumed to be contained between the walls of a hollow cylinder which has boundaries that are linear functions of time. It is shown that the presence of the ambient gas can be ignored in the qualitative descriptions of the flow determined from interferograms. Studies of the single and multiple fringe interferograms expected from such a cylindrical flow are made. Graphical plotting techniques are developed to obtain these expected interferograms, and supplementary mathematical relations describing the interferograms are demonstrated. Finally, comparison of interferograms obtained by these methods is made with those interferograms obtained during actual exploding wire experiments.

TABLE OF CONTENTS

LIST OF ILLUSTRATIONS

I. INTRODUCTION

Single and multiple fringe interferograms have been in use in recent years to obtain gas and electron distributions about an exploding wire[1]*. Until recently not much quantitative evidence has been obtained about the flow of the metal in these exploding wires. The purpose of this paper is to establish some geometrical techniques and mathematical relations upon which subsequent analyses of this metal flow, seen in the existing interferograms, may be based. This paper offers certain flow hypotheses, shows the resulting fringe contours for both the single and multiple fringe cases, and compares these fringe contours with some actual interferograms.

II. FLOW HYPOTHESES

A. Outer Zone Cases.

Figure 1 represents the expansion as a function of time of the boundaries of the metal vapor from a wire exploding in the presence of a low pressure gas. We assume this flow to be cylindrically symmetric about the wire axis. Gas density, ρ_o, is assumed constant for $r > r_M$. In the shocked ambient gas such that $r_M \geq r > r_N$ the approximate, constant value $4\rho_o$ is assumed. For $r_N \geq r \geq r_P$ the metal vapor is represented by constant density ρ_H ; and for the innermost region, where $r_P > r \geq 0$, density is taken to be zero. Note that all of the boundaries are assumed to be linear and intersect the r axis at time zero. This approximation fits the observed flow boundaries fairly closely and presents no serious problems except near $t = 0$. Thus ρ_H can be represented approximately as a hollow cylinder of metal vapor of inner radius $r_P = az$ and outer radius $r_N = bz$. Axial distance is related to time through the equation $z \cong 2\ell\omega t$, ω being the angular velocity of a mirror making the streak photograph of the event represented in Figure 1, ℓ is the optical lever arm, and t is the time elapsed since the initiation of the explosion[2]. If mass is conserved,

*References are listed on page 30.

and the original radius and density of the wire are represented by r_w and ρ_w respectively, then $\rho_H = \rho_w r_w^2/(b^2-a^2)\, z^2$, for $r_w \ll r$. The expression for a fringe shift δ at radius r_i, for rays which are normal to the r - z plane of a cylindrically symmetric disturbance of outer radius r_o, is given by [3]

$$\delta(r_i,z) = \frac{2}{\lambda^*} \int_{r_i}^{r_o} \frac{(n-n_o)s\,ds}{(s^2-r_i^2)^{\frac{1}{2}}} \tag{1}$$

where s is the radial distance to a point on the ray passing through the disturbance at r_i, n is the index of refraction at s, n_o is the index of refraction of the medium in the reference beam[2], and λ^* is the vacuum wavelength of the light used. For the disturbance assumed in Figure 1, n is not a function of s, and the integration may easily be carried out between the limits indicated in Figure 1, with the result

$$\frac{\lambda^*}{2z}\,\delta(r_i,z) = K_M\left(\frac{\rho_w r_w^2}{(b^2-a^2)z^2} - \rho_o\right)\left[(b^2-\alpha^2)^{\frac{1}{2}} - (a^2-\alpha^2)^{\frac{1}{2}}\right]$$

$$+ K_S\rho_o[3(c^2-\alpha^2)^{\frac{1}{2}} - 3(b^2-\alpha^2)^{\frac{1}{2}} - (a^2-\alpha^2)^{\frac{1}{2}}] \tag{2}$$

where in each zone the Dale-Gladstone approximation relating density and index of refraction has been made. The Dale-Galdstone constant used for the vacuum and ambient compressed gas zones is K_S, and K_M is used for the metal vapor zone. The parameter $\alpha = r/z$ has been introduced for convenience. Assuming that ρ_o is the density of 1/16 atm argon, that $K_S = K_M$, and that the values for a, b, and c are as shown in Figure 2, one may plot the (r,z) contour for a given fringe shift, e.g., $\delta = 6$, by solving Eq. (2) for z, calculating z as a function of α's of interest ($c \geq \alpha \geq 0$), and recalling $r = \alpha z$. This procedure results in the solid curves of Figure 2 for an r_w of 5 mils. The inner solid curve represents the negative root of z, the outer the positive root.

B. Approximation to Outer Zone Case.

Because $\rho_w r^2/(b^2-a^2)z^2 \gg \rho_o$ and the bracketed radicals are all of the same order of magnitude for the experiments performed, we might reasonably assume that the effect on δ of the outer zone and inner vacuum zone is small. With this assumption, Eq. (2) may be written

$$\delta = \frac{2K_M r_w^{\,2} \rho_w}{\lambda*(b^2-a^2)z} \left[(b^2-\alpha^2)^{\frac{1}{2}} - (a^2-\alpha^2)\right]^{\frac{1}{2}} . \tag{3}$$

Following the same plotting procedure and using the same numerical fringe shift number as before, Eq. (3) yields the dashed curve in Figure 2. The adjacent solid curve is quite similar in shape to the dashed curve, differing only in magnitude. Defining the difference between ordinate values for the two lower curves as Δr, it can be shown that at a fixed z as $\delta \to \infty$, Δr monotonically approaches 0. Because the δ chosen in the figure ($\delta = 6$) is small compared to those likely to occur in actual experiments, the difference between the lower curves is about the largest that might be expected. Since this difference is reasonably small, the use of Eq. (3) in place of Eq. (2) is assumed to be justified in representing the lower curves. The (r,z) contour from Eq. (3) does not have an outer curve to compare with that from Eq. (2). In any case the outer curve does not occur at z values of current interest ($z < 5$ cm), nor has it been observed experimentally. Consequently, the fact that Eq. (3) yields no outer curve is not considered a serious shortcoming in its use in preference to Eq. (2). We will use Eq. (3) therefore in subsequent discussions.

III. GEOMETRICAL CONSTRUCTION

A. The Function $G(\alpha)$

Defining the bracketed term of Eq. (3) as $G(\alpha)$, we recall how the function is generated. In Figure 3 for $0 \le \alpha \le a$, $G(\alpha)$ is represented as the length of the line cd, which is the difference in ordinate values for two circles of radius a and b and abscissa α. For $a \le \alpha \le b$,

$G(\alpha)$ can be represented as the ordinate distance to the radius b circle. Hence

$$G(\alpha) = (b^2-\alpha^2)^{\frac{1}{2}} - (a^2-\alpha^2)^{\frac{1}{2}}, \qquad 0 \le \alpha \le a$$
$$= (b^2-\alpha^2)^{\frac{1}{2}}, \qquad a \le \alpha \le b. \tag{4}$$

$G(\alpha)$ versus α is also shown in Figure 3 as the heavy curve. Note that $G_{max} = (b^2-a^2)^{\frac{1}{2}}$, $G(0) = b - a$, and $G(b) = 0$. One can easily verify that $G'(a) = +\infty$, $G'(b) = -\infty$, and $G'(0) = 0$ as shown in the figure.

B. Single Fringe Construction.

From Eqs. (4), Eq. (3) may be written as

$$z = KG(\alpha)/\delta \tag{5}$$

where the definition of K is evident by inspection. Keeping δ fixed, one may plot the lines $r = \alpha z$ and $z = KG(\alpha)/\delta$ for all α's of interest. Where these curves intersect for the same α is a point in the r - z plane for the chosen fringe shift δ. The locus of intersection points therefore describes the fringe shift contour in the r - z plane. Such a geometrical procedure is followed in Figure 4, where the bottom abscissa represents the quantity $KG(\alpha)/\delta$. The fringe shift contour is traced out in the top half of the figure. Fringe shift patterns of this type are frequently observed experimentally. Figure 5 is a single fringe interferogram of a copper wire exploded in 1/8 atm. argon. The wing-like structure of Figure 4 is apparent in the region of Figure 5 close to the $r = 0$ axis.

Interferograms of wires exploded in a vacuum indicate the absence of the inner boundary defined by the line $r = az$, i.e., the expansion takes the form of a solid cylinder with a radius that is increasing linearly with time. Figure 6 is an interferogram of this vacuum explosion. It should be compared with Figure 7 which is a plot of Eq. (3) for $a = 0$, $b = 1$.

C. Multiple Fringe Interferograms.

The fringe shift δ is given by $\delta = r/W - r_0/W$ where r is the radius of the fringe in the disturbed region, and r_o is the radius of the same fringe in the undisturbed region. Fringes in the undisturbed region are aligned parallel to the z axis and equally spaced a distance W apart. Then from Eq. (5)

$$(r - r_o)z = KWG(\alpha). \tag{6}$$

Dividing Eq. (6) by $|r_o|$ and defining $\bar{r} \equiv r/|r_o|$ and $\bar{z} \equiv z/|r_o|$, yields

$$(\bar{r} \mp 1)\bar{z} = KWG(\alpha)/r_o^2. \tag{7}$$

The upper sign represents the case where $r_o > 0$, the lower where $r_o < 0$. Also

$$\bar{r} = \pm x\bar{z} , \tag{8}$$

where $x \equiv |\alpha|$.

Eq. (7) represents equilateral hyperbolae with origins at $\bar{r} = \pm 1$, $\bar{z} = 0$. Note that with such hyperbolae the radial distance between the origin and the hyperbola measured along the $(\bar{r} \mp 1) = \bar{z}$ line is given by $(2KWG/r_o^2)^{\frac{1}{2}}$. Thus for $r_o > 0$, one may plot Eq. (7) for a given α, r_o, K and W and obtain a hyperbola in the $\bar{r}$ - $\bar{z}$ plane. One may also plot Eq. (8) and the intersection point of this straight line with the hyperbola corresponds to the value of (r, z) for the α chosen. Selecting all α's of interest, one may thus determine the contour of a fringe as it passes through the region of disturbance. This procedure is followed in Figure 8. On the inclined axis the radial distance is plotted versus α. Figure 9 is a multiple fringe interferogram taken in the presence of argon at 1/16 atmosphere. The hook-like behavior of the fringe in Figure 8 can be seen in the fringes of the upper portion of Figure (9).

A similar plotting treatment for $r_o < 0$ is carried out in Figure 10. In this case there are two branches of the fringe contour corresponding to two points of intersection of Eqs. (7) and (8). For some values of α these two branches may intersect as shown in Figure 11 to form an "excluded region", i.e., a region where for a particular range of α, no fringes can occur. Geometrically, this results from the abscissa values of a set of hyperbolae being everywhere greater than those for the corresponding set of $\bar{r} = -x\bar{z}$ lines, i.e., no intersection occurs. Evidence of this excluded region has not been found experimentally.

IV. MATHEMATICAL RELATIONSHIPS

A. Single Fringe Case.

From Eqs. (4) and (5)

$$\frac{dr}{dz} \equiv \frac{dr/d\alpha}{dz/d\alpha} = \alpha + \frac{1}{\alpha}\left[(b^2-\alpha^2)(a^2-\alpha^2)\right]^{\frac{1}{2}}, \qquad 0 \le \alpha \le a$$

$$= \frac{(2\alpha^2-b^2)}{\alpha}, \qquad a < \alpha \le b. \tag{9}$$

Hence for single fringe interferograms

$$\frac{dr}{dz} = a,\ b,\ +\infty, \text{ at } \alpha = a,\ b,\ 0, \text{ respectively.}$$

These slope values correspond qualitatively to those of the single fringe interferogram of Figure 5.

B. Multiple Fringe Case.

From Eqs. (7) and (8) one may solve for $\bar{z}$ and obtain

$$\bar{z} = \frac{(-1)^i + (-1)^j P^{\frac{1}{2}}}{(-1)^k\, 2x}, \tag{10}$$

where $P = 1 + (-1)^k 4GWKx/r_o^2$. The values for the possible fringes, seen in composite in Figure 12, are given in Table I.

Table I. Matrix of Indices

Region	i	j	k	Fringe
$r_o > 0, \bar{r} > 0$	even	even	even	I
$r_o > 0, \bar{r} > 0$	even	odd	even	not allowed
$r_o > 0, \bar{r} < 0$	even	even	odd	not allowed
$r_o > 0, \bar{r} < 0$	even	odd	odd	not allowed
$r_o < 0, \bar{r} > 0$	odd	even	even	II
$r_o < 0, \bar{r} > 0$	odd	odd	even	not allowed
$r_o < 0, \bar{r} < 0$	odd	even	odd	III
$r_o < 0, \bar{r} < 0$	odd	odd	odd	IV

When k is odd, Eq. (10) has imaginary roots when $1 < 4\ GWKx/r_o^2$. This means no representation in the real $\bar{r} - \bar{z}$ plane. These imaginary roots correspond to the "excluded regions" of Figure 11. Note that at the boundaries of the excluded regions.

$$1 = 4GWKx/r_o^2 \qquad (11)$$

so that the upper and lower branch always intersect at $\bar{r} = -1/2$.

The slope $d\bar{r}/d\bar{z}$ can be determined as in Eq. (9). The result is

$$\frac{d\bar{r}}{d\bar{z}} = \frac{2x^2 M}{(-1)^k 2xM - P + (-1)^{i+j+1} P^{\frac{1}{2}}}\ , \qquad (12)$$

where

$$M(x) \equiv (KW/r_o^2)\ d(xG)/dx\ .$$

The values for i, j, k for a given fringe are again found in Table I. Hence at the intersection of the upper and lower branches of the curve below $\bar{r} = 0$ line, $d\bar{r}/d\bar{z} = -x_1, -x_2$, where x_1 and x_2 are roots of Eq. (11). Also $d\bar{r}/d\bar{z} = (-1)^k|a|, (-1)^k|b|$, at $x = |a|, |b|$, respectively. Also for both curves II and III

$$\left.\frac{d\bar{r}}{d\bar{z}}\right|_{x=0} = \frac{-r_0}{KW}\,\frac{1}{(b-a)} \,. \qquad (13)$$

Comparing this value with that of the slope for single fringe interferograms, we see that the two slopes of the single and multiple fringe interferograms can never be equal at x = 0.

C. Asymptotic Behavior.

The shape of the fringe for large $\bar{z}$ for the multiple fringe case can be seen from Eqs. (8) and (10). Combining these

$$\bar{r}(x) = \frac{(-1)^i + (-1)^j P^{\frac{1}{2}}}{2} \qquad (14)$$

where i, j, and k are even or odd integers as given in Table I, $\bar{r}(x)$ at $\bar{z} = \infty$ is given by $\bar{r}(0)$. For the curve of Figure 8, curve I, $(r_0 > 0)$ i and j are even integers hence $\bar{r}(0) = 1$. That is, the fringe after passing through the region of disturbance will asymptotically approach its initial configuration, i.e., a line parallel to the $\bar{r} = 0$ axis at a distance of unity away from the axis.

Likewise for the lowermost curves of Figure 10, curve IV, $(r_0 < 0)$ i and j are odd. Hence from Eq. (14), $\bar{r}(0) = -1$. The lowermost curve thus approaches its initial position with increasing $\bar{z}$. This asymptotic behavior for $r_0 \lessgtr 0$ is discernible in the multiple fringe interferogram Figure 9.

We examine the behavior of the closed branch of Figure 10 made up of curves II and III for the case where $|\bar{r}| \ll 1$. From Eq. (14), and the definition of P, asserting $|r| \ll 1$ implies $1 \gg 4xGWK/r_0^2$. Thus $P^{\frac{1}{2}}$

may be expanded and only the first few terms need be retained. Eq. (14) then becomes

$$\bar{r} \approx \pm \frac{xGWK}{r_o^2} - \frac{2x^2W^2G^2K^2}{r_o^4} . \tag{15}$$

The upper sign refers to the portion above the $\bar{r} = 0$ axis, the lower sign to the portion below. From the definitions of δ, and $\bar{r}$, one may write for curves II and III

$$\frac{\delta}{|r_o|} = \frac{\bar{r}}{W} + \frac{1}{W} \approx \frac{1}{W} , \tag{16}$$

for $|\bar{r}| \ll 1$. Hence, Eq. (15) may be written

$$\bar{r} \approx \pm \frac{xGK}{\delta|r_o|} - \frac{2x^2G^2K^2}{\delta^2 r_o^2} . \tag{17}$$

From Eqs. (5) and (8) the $\bar{r}$ variation of a fringe of the single fringe type is given by

$$\bar{r} = \pm \frac{xGK}{\delta|r_o|} . \tag{18}$$

Note that a comparison of Eqs. (17) and (18) shows that the dependence on x of the first terms of both equations is the same. That is, for small $\bar{r}$'s, the inner closed branch should be similar to the single fringe in appearance. This resemblance is seen in Figures 4 and 10. The higher order terms of Eq. (17) cause the distortion noted in Figure 10, making the $\bar{r}$ values above the axis less positive, and those below more negative. There is some suggestion of this single-fringe-like closed loop near the axis at the beginning of the expansion in Figure 9. However, the processes occuring there may be very complex, and the simple assumptions resulting in the closed loop of Figure 10 are very tenuous.

V. CONCLUSIONS

In flow studies of metal vapor from a wire exploded in argon at low density, the effect of the shocked gas outer regions can be neglected in the qualitative analysis of the resulting interferogram.

Single fringes of the type depicted in Figure 4 are similar to those obtained experimentally and shown in Figure 5. Thus, the assumption that the vapor expands in a hollow cylinder with boundaries that are linear functions of time is sufficient to explain the single fringe behavior observed for wires exploded in low density argon. Likewise the fringes of Figure 7 are very similar to those obtained experimentally and shown in Figure 6, and it is sufficient in explaining the behavior of the interferograms of the wires exploded in a vacuum to assume a solid cylindrical expansion with an outer boundary that is a linear function of time.

Multiple fringes of the type seen in Figure 9 are similar to those obtained experimentally and shown in Figure 8, lending further credence to the expanding cylinder model for the explosion.

Fringes of the multiple interferograms may have closed inner loops similar to those of the single fringe type, and Figure 9 may show some evidence of this similarity.

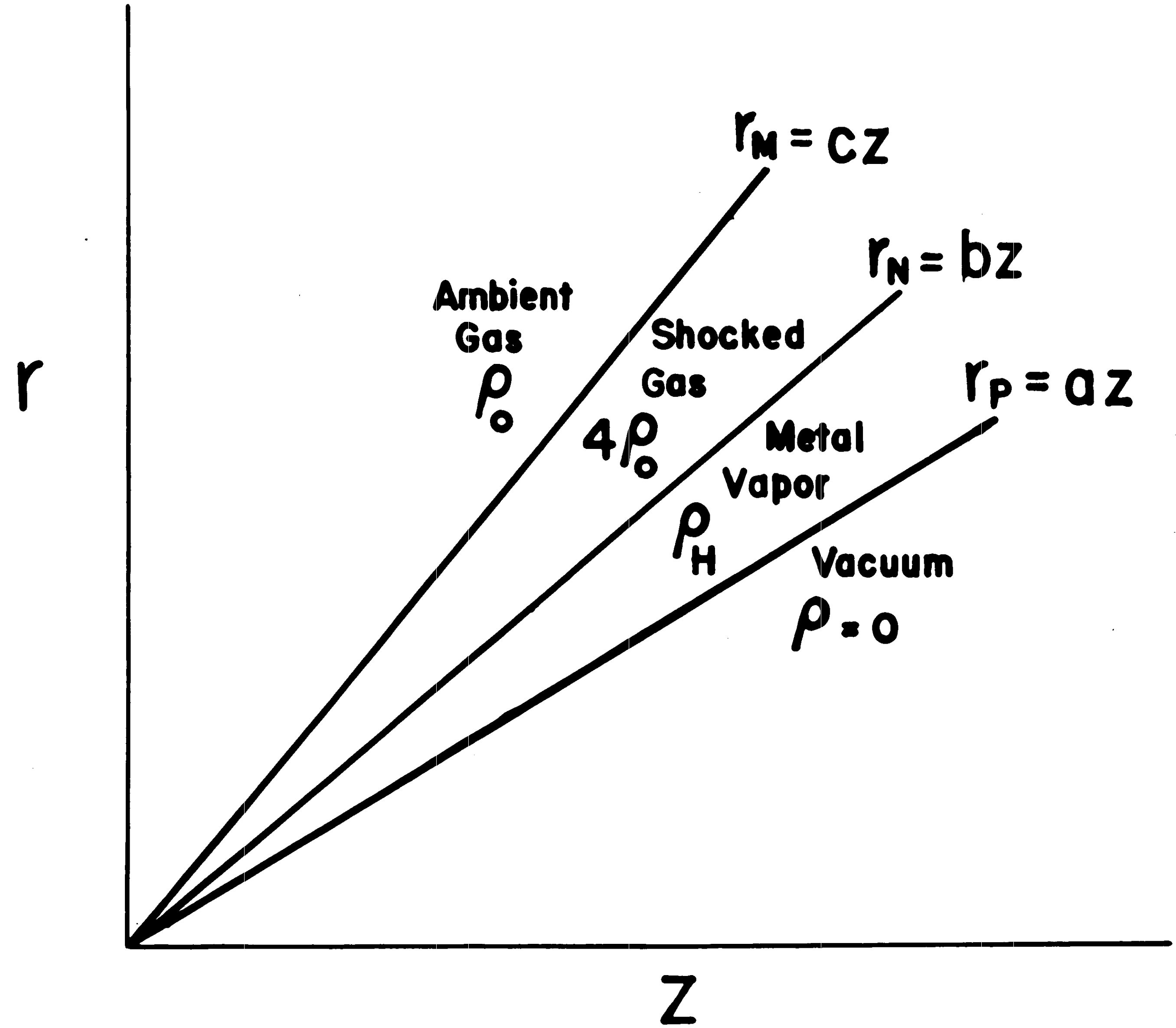

Figure 1. Flow Assumed in Vaporization Process

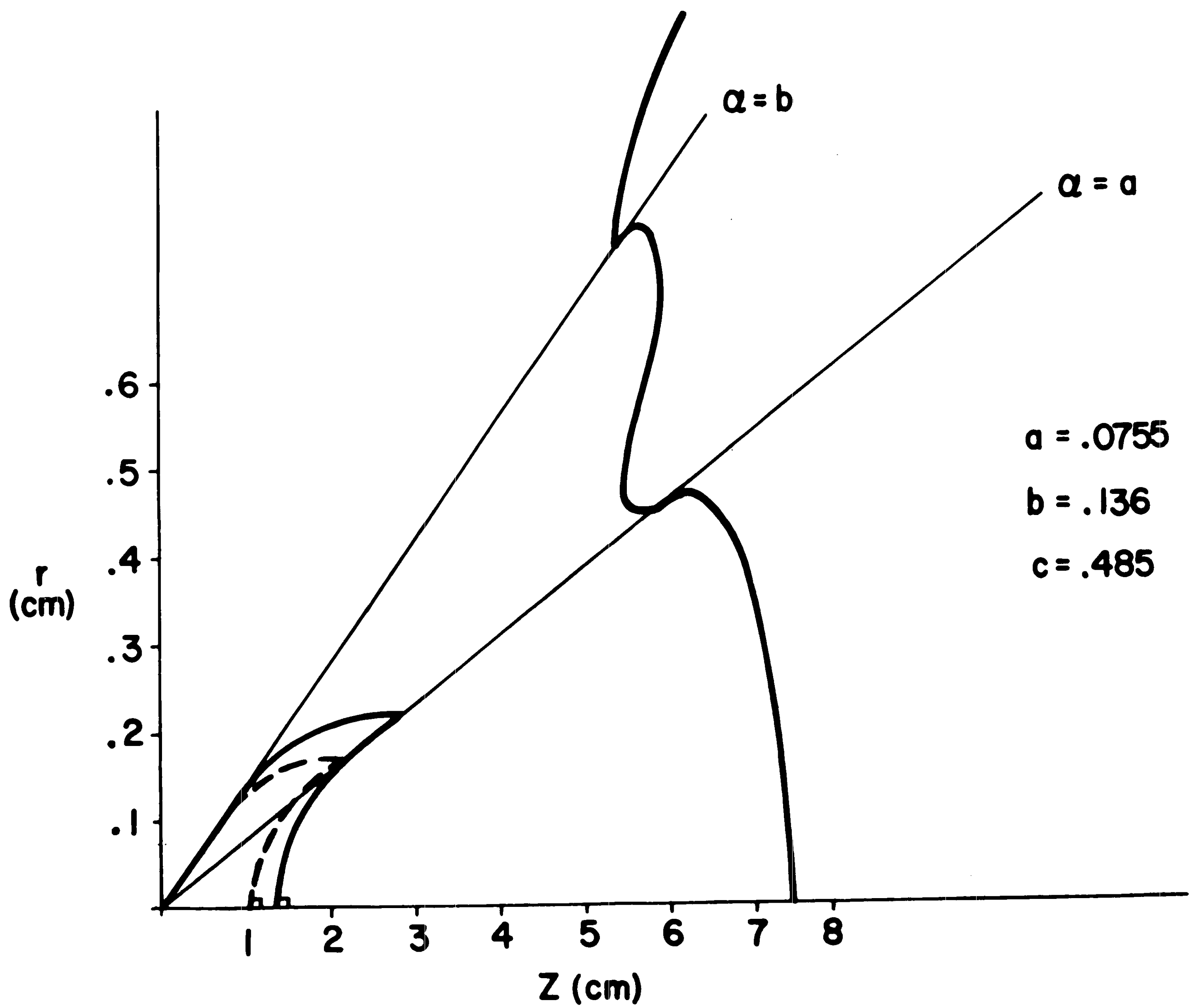

Figure 2. Plots of Fringe Shapes Expected from the Flow Assumptions of Figure 1

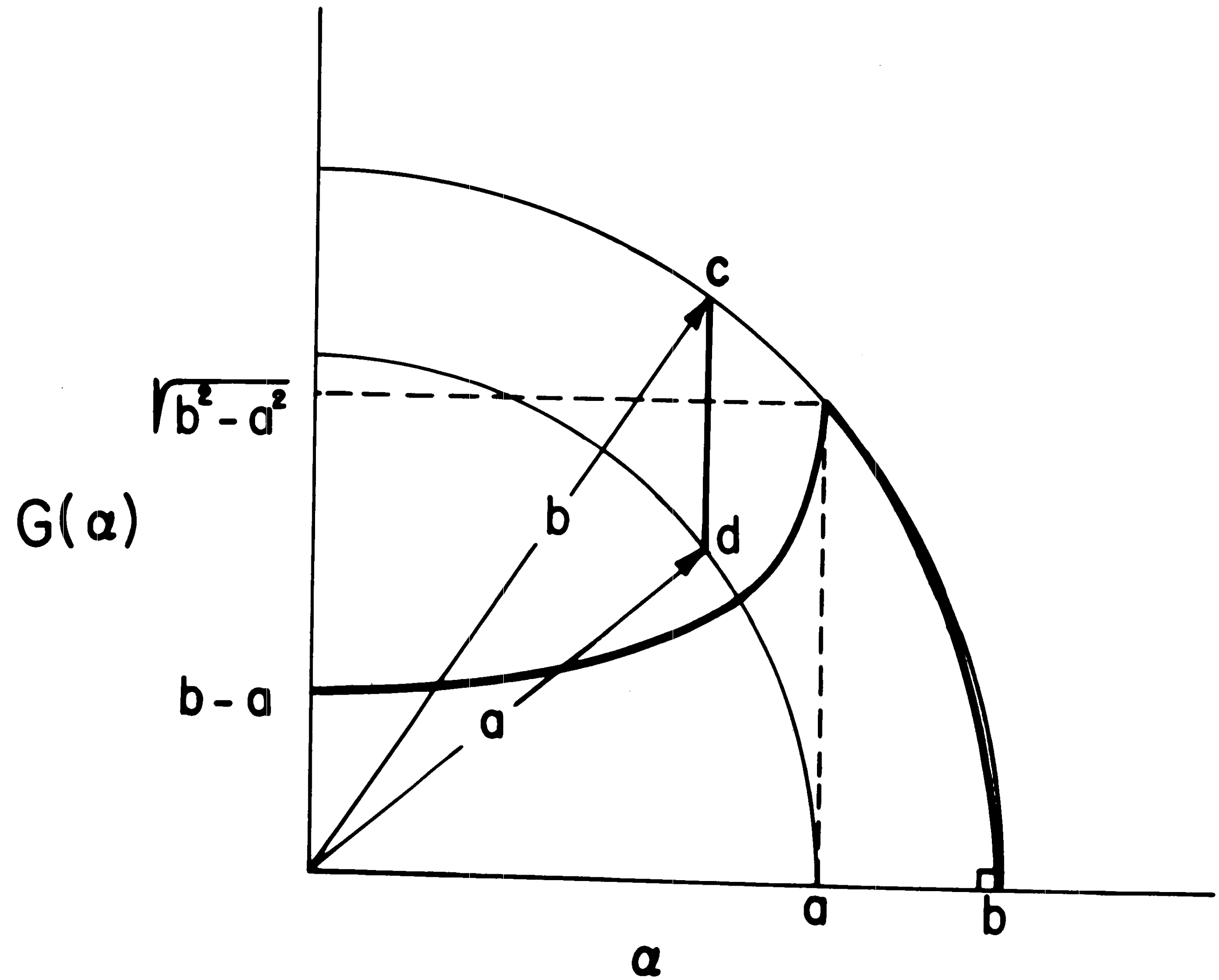

Figure 3. A Plot of the Function $G(\alpha)$

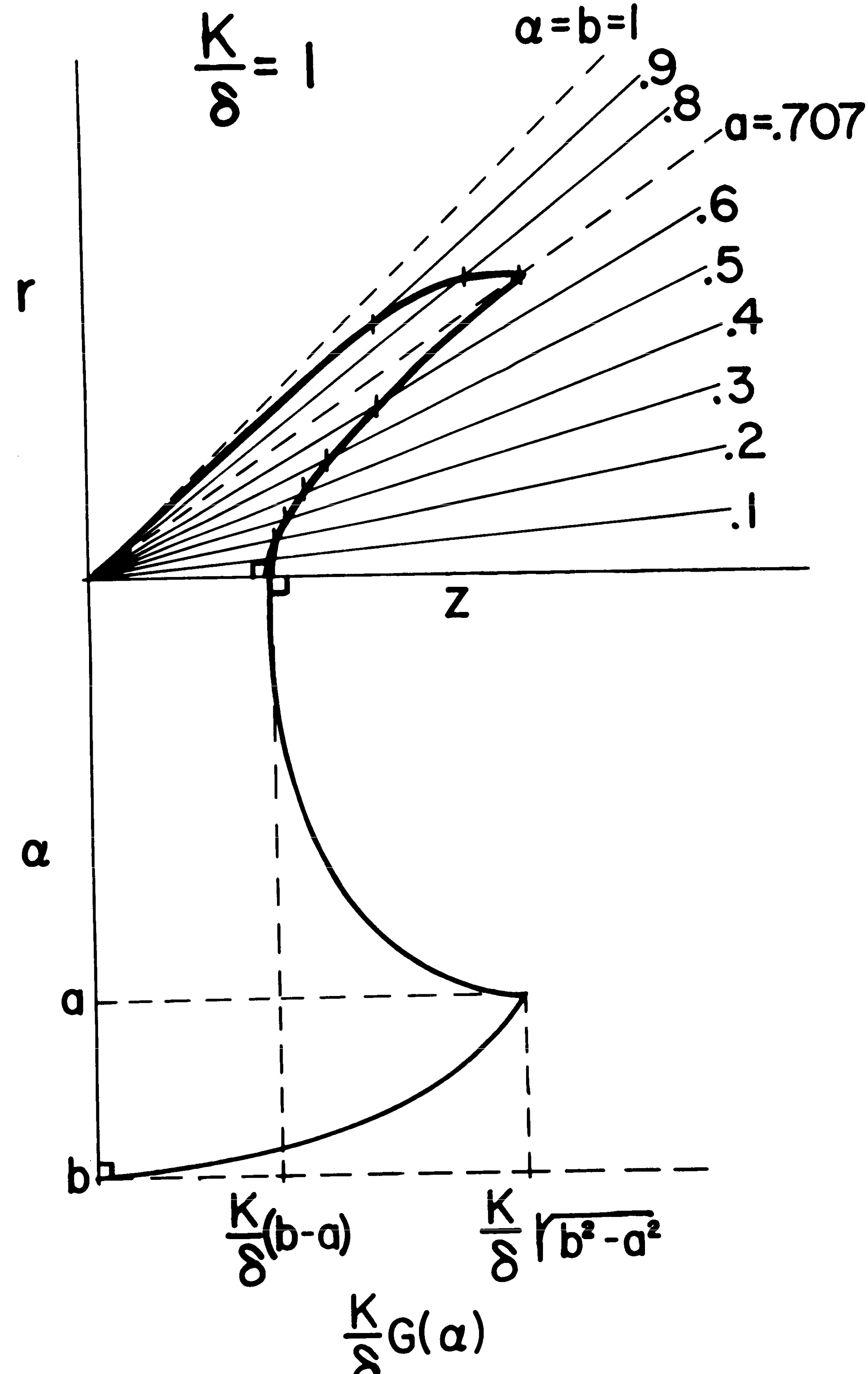

Figure 4. Single Fringe Construction. Where a = 0.707 and b = 1

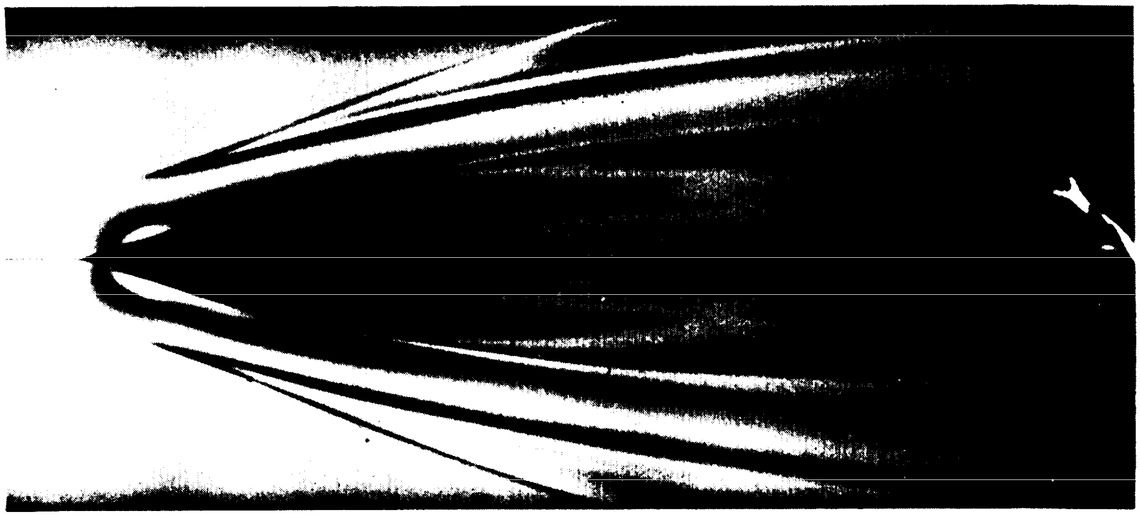

Figure 5. Single Fringe Interferogram of Cu Wire Exploded in 1/8 atm Argon

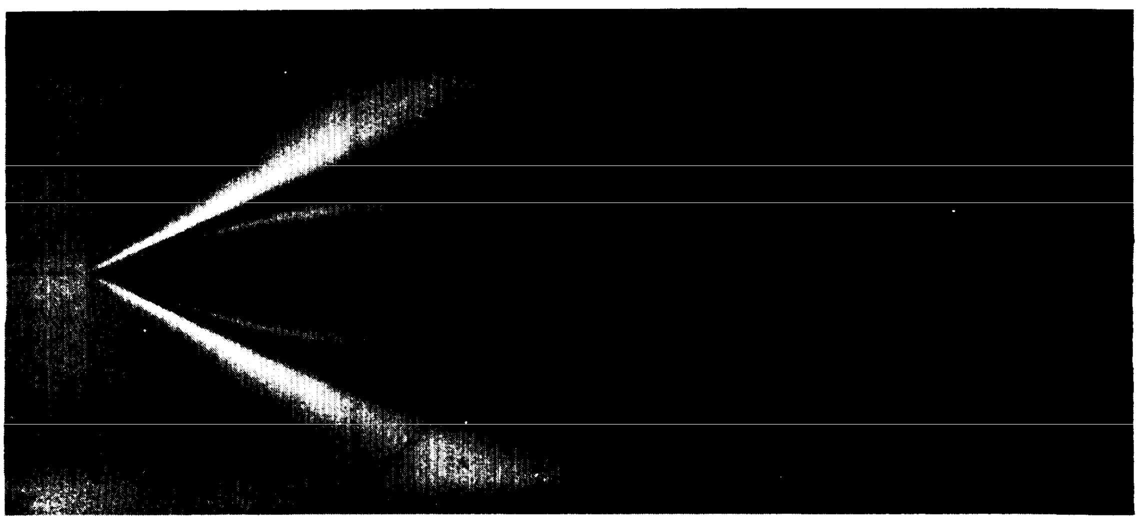

Figure 6. Single Fringe Interferogram of Cu Wire Exploded in a Vacuum

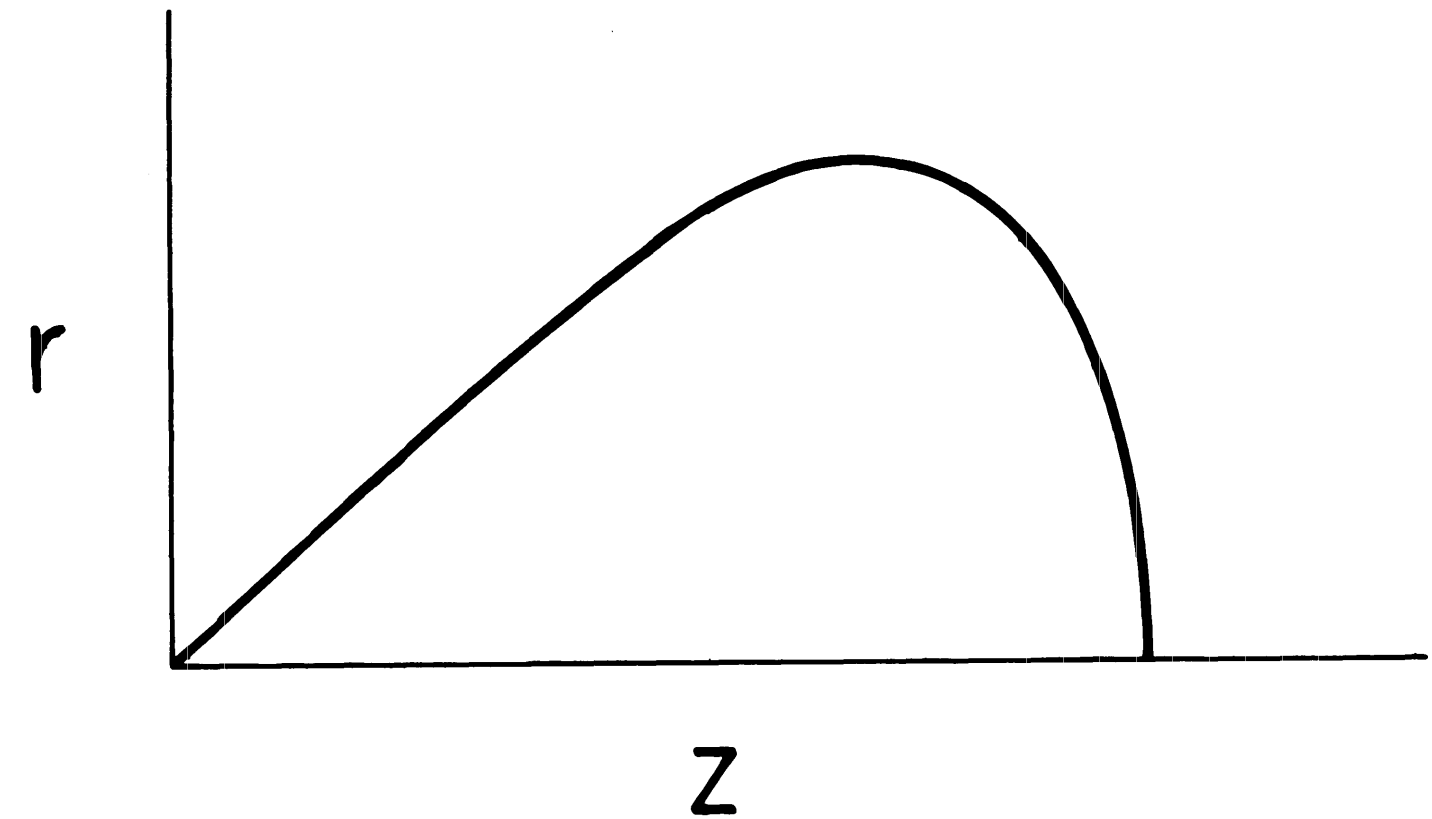

Figure 7. Single Fringe Interferogram for a = 0, b = 1, and $K/\delta = 1$

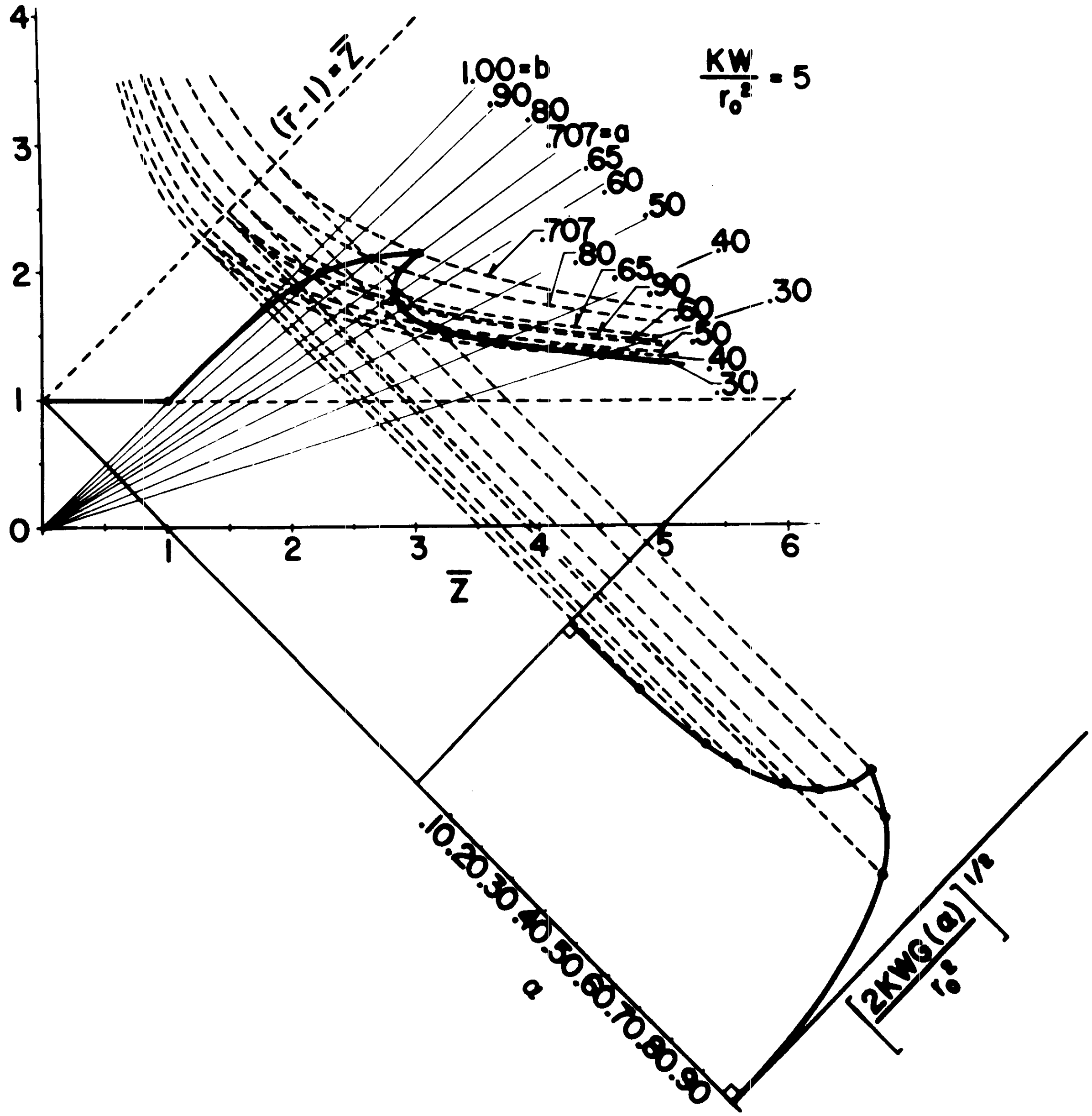

Figure 8. Multiple Fringe Interferogram Construction for the $\bar{r} > 0$ Case

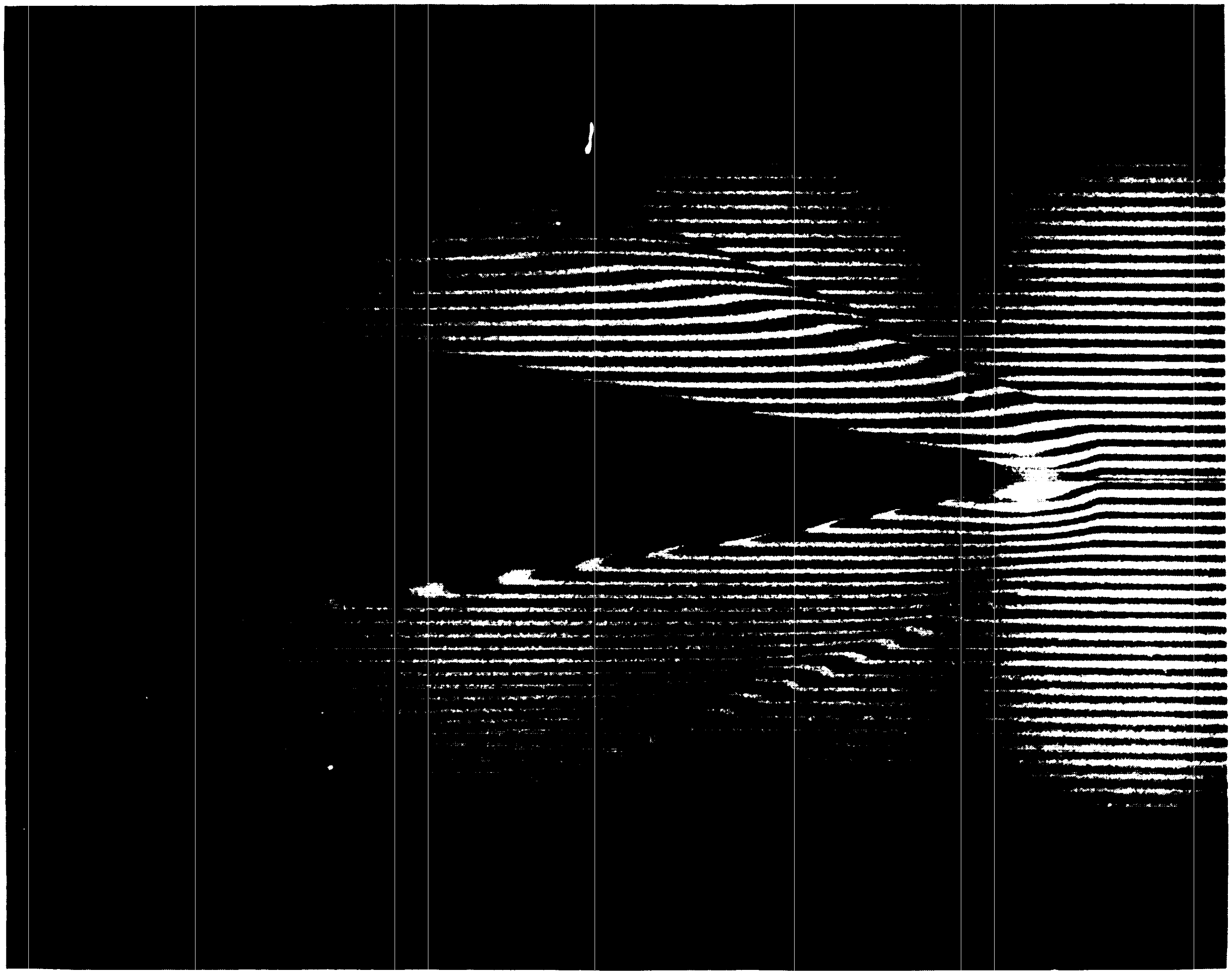

Figure 9. Multiple Fringe Interferogram for Cu Wire Exploded in 1/16 atm Argon

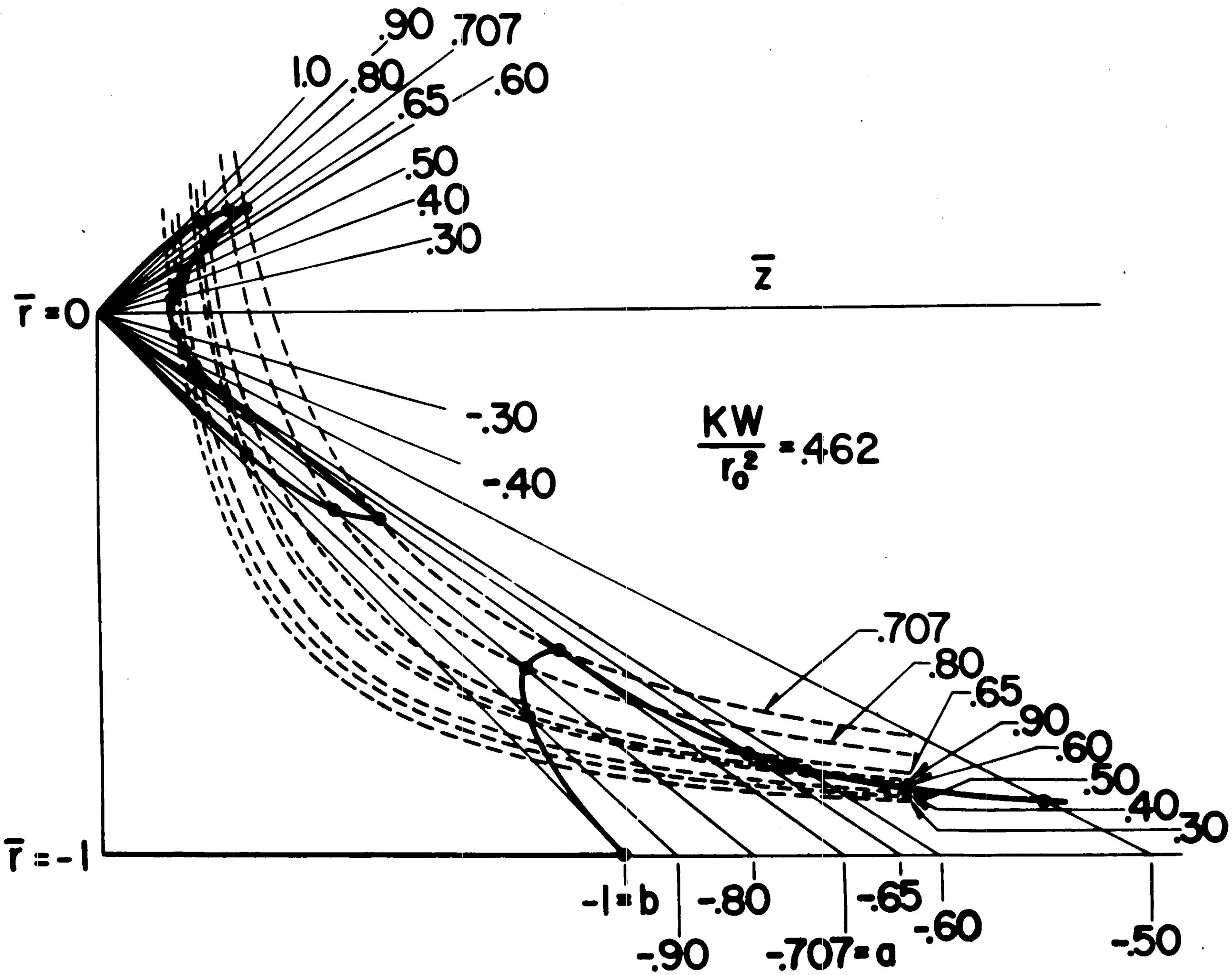

Figure 10. Fringe Construction for $r_o < 0$ Case

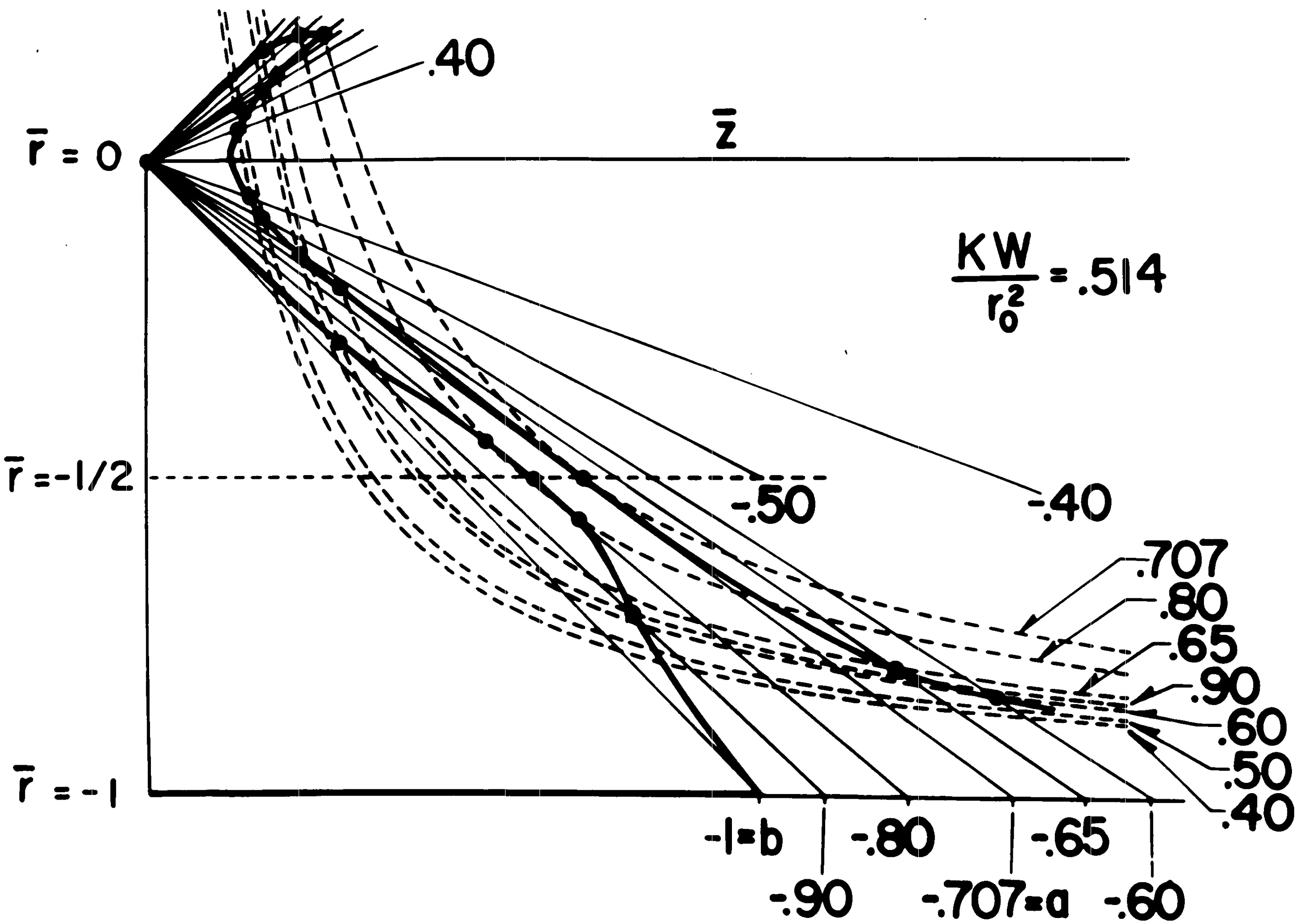

Figure 11. Fringe Construction Showing Excluded Region

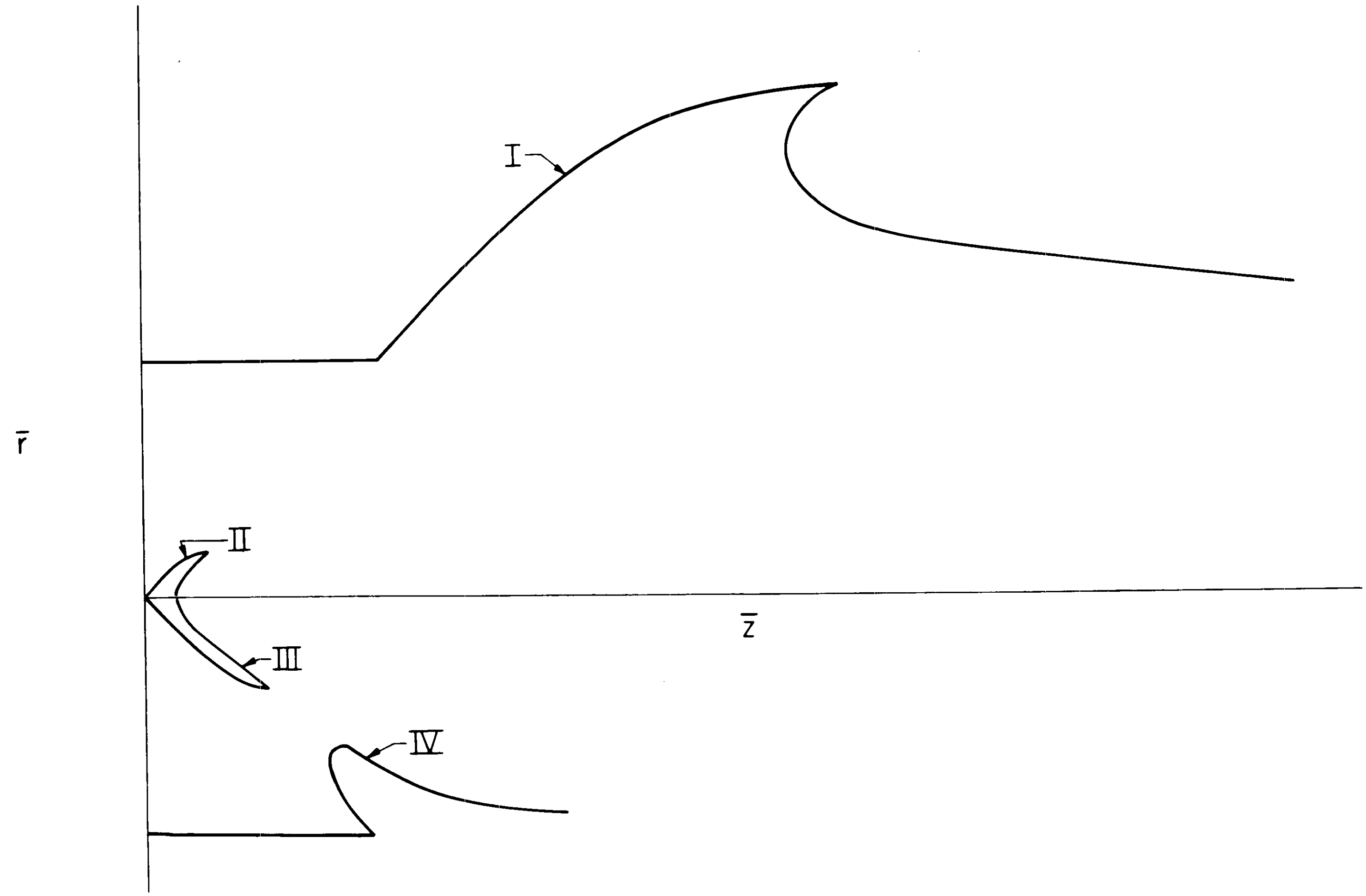

Figure 12. Composite Showing Fringe Constructions Possible for Multiple Fringe Interferograms

REFERENCES

1. G. D. Kahl and E. H. Wedemeyer, Phys. of Fluids 7, 596 (1964).

2. F. D. Bennett, H. S. Burden, and D. D. Shear, Phys. of Fluids 5, 102 (1962).

3. F. D. Bennett, W. C. Carter and V. E. Bergolt, J. of Appl. Phys. 23, 453 (1952).

DISTRIBUTION LIST

No. of Copies	Organization
20	Commander Defense Documentation Center ATTN: TIPCR Cameron Station Alexandria, Virginia 22314
1	Commanding General U.S. Army Materiel Command ATTN: AMCRD-TE Washington, D.C. 20315
1	Commanding General U.S. Army Materiel Command ATTN: AMCRD-TP Washington, D.C. 20315
1	Commanding General U.S. Army Materiel Command ATTN: AMCRD-BN Washington, D.C. 20315
2	Commanding General U.S. Army Missile Command ATTN: AMSMI-RBL Redstone Arsenal, Alabama 35809
1	Commanding Officer U.S. Army Mobility Equipment Research & Development Center ATTN: Docu Ctl Ctr, Bldg 315 Fort Belvoir, Virginia 22060
2	Commanding Officer U.S. Army Frankford Arsenal ATTN: SMUFA-N1000 Mr. C. Lukens SMUFA-C2500 Philadelphia, Pennsylvania 19137

No. of Copies	Organization
1	Commanding Officer U.S. Army Picatinny Arsenal ATTN: SMUPA-V Mr. E. Walbrecht Dover, New Jersey 07801
1	Commanding Officer U.S. Army Harry Diamond Laboratories Washington, D.C. 20438
1	Commandant U.S. Army Logistics Management Center Fort Lee, Virginia 23801
1	Commanding Officer U.S. Army Materials and Mechanics Research Center Watertown, Massachusetts 02172
1	Commanding General U.S. Army Natick Laboratories Natick, Massachusetts 01762
1	Commanding Officer U.S. Army Foreign Science & Technology Center Munitions Building Washington, D.C. 20315
1	Commanding Officer U.S. Army Cold Regions Research and Engineering Laboratories Hanover, New Hampshire 03755
1	Commanding Officer U.S. Army Satellite Communications Agency Fort Monmouth, New Jersey 07703

DISTRIBUTION LIST

No. of Copies	Organization
1	Commanding Officer U.S. Army Maintenance Board Fort Knox, Kentucky 40121
1	Commanding General U.S. Army Combat Developments Command ATTN: CDCMR-W Fort Belvoir, Virginia 22060
1	Office of Vice Chief of Staff ATTN: CSAVCS-W-TIS Department of the Army Washington, D.C. 20310
1	Director U.S. Army Research Office 3045 Columbia Pike Arlington, Virginia 22204
1	Commanding Officer U.S. Army Research Office (Durham) Box CM, Duke Station Durham, North Carolina 27706
3	Commander U.S. Naval Air Systems Command ATTN: AIR-604 Washington, D.C. 20360
3	Commander U.S. Naval Ordnance Systems Command ATTN: ORD-9132 Washington, D.C. 20360
1	Commander U.S. Naval Weapons Center ATTN: Code 753 China Lake, California 93555
2	Commander U.S. Naval Ordnance Laboratory ATTN: Code 730, Lib Code 242 Mr. H. Leopold Silver Spring, Maryland 20910
1	Superintendent U.S. Naval Postgraduate School ATTN: Tech Rept Sec Monterey, California 93940
3	Director U.S. Naval Research Laboratory ATTN: Code 7700, Dr. A. Kolb Code 7720 Dr. E. McLean Mr. I. Vitkovitsky Washington, D.C. 20390
1	Commander U.S. Naval Weapons Laboratory Dahlgren, Virginia 22448
1	ADTC (ADBPS-12) Eglin AFB Florida 32542
1	ADTC (ADOW) Eglin AFB Florida 32542
1	AFATL (ATW) Eglin AFB Florida 32542
1	AFWL (WLRE, Dr. Guenther) Kirtland AFB New Mexico 87117
1	AUL (3T-AUL-60-118) Maxwell AFB Alabama 36112

DISTRIBUTION LIST

No. of Copies	Organization
1	AFAL (AVW) Wright-Patterson AFB Ohio 45433
3	Director National Bureau of Standards ATTN: Dr. D. Tsai Mr. P. Krupenie Mr. J. Park U.S. Department of Commerce Washington, D.C. 20235
1	Headquarters U.S. Atomic Energy Commission ATTN: Lib Br Washington, D.C. 20545
1	Manager U.S. Atomic Energy Commission Depository Library Gmelin Institute ATTN: Mr. B. Baschkin 193 Mulberry Lane Larchmont, New York 10538
3	Director U.S. Atomic Energy Commission ATTN: Tech Info Div P.O. Box 62 Oak Ridge, Tennessee 37831
1	Director Lawrence Radiation Laboratory ATTN: Dr. C. Olsen P.O. Box 808 Livermore, California 94550
2	Director Los Alamos Scientific Laboratory ATTN: Dr. R. Reithel Dr. J. L. Tuck P.O. Box 1663 Los Alamos, New Mexico 87544

No. of Copies	Organization
1	Director NASA Scientific & Technical Information Facility ATTN: SAK/DL P.O. Box 33 College Park, Maryland 20740
1	Director National Aeronautics and Space Administration Electronics Research Center ATTN: Dr. V. Scherrer 575 Technology Square Cambridge, Massachusetts 02139
1	Director National Aeronautics and Space Administration Langley Research Center ATTN: Code 04.000 Langley Station Hampton, Virginia 23365
1	Director National Aeronautics and Space Administration Lewis Research Center 21000 Brookpark Road Cleveland, Ohio 44135
1	Director Jet Propulsion Laboratory ATTN: Mr. I. Newlan 4800 Oak Grove Drive Pasadena, California 91103
1	Director Smithsonian Astrophysical Observatory 60 Garden Street Cambridge, Massachusetts 01238

DISTRIBUTION LIST

No. of Copies	Organization
1	Aerojet-General Corporation ATTN: Dr. G. Woffinden 11711 South Woodruff Avenue Downey, California 90241
1	Atlantic Research Corporation ATTN: Mr. A. Macek Shirley Highway at Edsall Road Alexandria, Virginia 22314
2	AVCO-Everett Research Laboratory ATTN: Tech Lib Dr. G. Sargent James 2385 Revere Beach Parkway Everett, Massachusetts 02149
1	E. I. duPont de Nemours and Company Eastern Laboratory Library ATTN: Miss M. Imbrie Gibbstown, New Jersey 08027
1	General Electric Research Laboratory ATTN: Dr. R. Alpher P.O. Box 1088 Schenectady, New York 12305
1	General Electric Company Space Sciences Laboratory ATTN: Dr. R. Good, Jr. P.O. Box 8555 Philadelphia, Pennsylvania 19101
1	Hughes Aircraft Company Systems Development Laboratory ATTN: Dr. A. Puckett Florence and Teale Streets Culver City, California 90230

No. of Copies	Organization
1	North American Rockwell Corporation Space Division ATTN: Dr. J. O'Keefe 12214 Lakewood Boulevard Downey, California 90241
1	Radio Corporation of America RCA Laboratories Division ATTN: Dr. H. Hendel Princeton, New Jersey 08540
1	Cornell Aeronautical Laboratory, Inc. ATTN: Dr. G. Skinner P.O. Box 235 Buffalo, New York 14221
1	Hartford Graduate Center R.P.I. ATTN: Prof. R. Campbell East Windsor Hill, Conn. 06028
1	Harvard University ATTN: Prof. H. Emmons Cambridge, Mass. 02138
1	University of Houston Department of Physics ATTN: Dr. D. Ross Cullen Boulevard Houston, Texas 77004
1	IIT Research Institute ATTN: Dr. Robert Dennen 10 West 35th Street Chicago, Illinois 60616
1	University of Illinois Department of Aeronautical Engineering Prof. R. Strehlow Urbana, Illinois 61803

DISTRIBUTION LIST

No. of Copies	Organization
1	Director Applied Physics Laboratory The Johns Hopkins University 8621 Georgia Avenue Silver Spring, Maryland 20910
1	The Johns Hopkins University Department of Mechanics ATTN: Prof. L. Kovasznay 34th and Charles Street Baltimore, Maryland 21218
1	Lehigh University Department of Physics ATTN: Prof. R. Emrich Bethlehem, Pennsylvania 18015
2	University of Maryland Institute of Fluid Dynamics and Applied Mathematics ATTN: Prof. J. Burgers Prof. S. Pai College Park, Maryland 20740
1	Willow Run Laboratories ATTN: Tech Docu Svcs P.O. Box 2008 Ann Arbor, Michigan 48104
1	University of Michigan Department of Physics ATTN: Prof. O. Laporte Ann Arbor, Michigan 48104
2	University of Michigan Gas Dynamics Laboratories ATTN: Mr. E. Oktay Prof. P. Sherman North Campus, Building 422 Ann Arbor, Michigan 48105
2	Sandia Corporation Livermore Laboratory ATTN: Mr. J. R. Hearst Building T105 Dr. G. Anderson P.O. Box 969 Livermore, California 94550
3	Sandia Corporation ATTN: Dr. E. Cnare Dr. F. Neilson Dr. T. Tucker P.O. Box 5800 Albuquerque, New Mexico 87115
1	Shock Hydrodynamics, Inc. ATTN: Dr. L. Zernow 15010 Ventura Boulevard Sherman Oaks, California 91403
1	Arizona State University ATTN: Prof. R. Stoner Tempe, Arizona 85281
1	University of Arkansas Department of Physics ATTN: Prof. O. Zinke Fayetteville, Arkansas 72701
1	California Institute of Technology Guggenheim Aeronautical Laboratory ATTN: Prof. L. Lees Pasadena, California 91104
1	California Institute of Technology Aeronautics Department ATTN: Prof. H. Liepmann 1201 East California Blvd. Pasadena, California 91102

DISTRIBUTION LIST

No. of Copies	Organization
1	California Institute of Technology Firestone Flight Sciences Laboratory ATTN: Prof. G. Whitham Pasadena, California 91104
1	Case Institute of Technology Department of Mechanical Engineering ATTN: Prof. G. Kuerti 10900 Euclid Avenue Cleveland, Ohio 44106
1	University of California Department of Chemistry ATTN: Dr. G. Nash Davis, California 95616
1	University of California Department of Mechanical Engineering ATTN: Prof. S. Schaaf Berkeley, California 94704
1	Columbia University ATTN: Prof. R. Gross 236 Seeley W. Mudd Building New York, New York 10027
1	University of Colorado Joint Institute for Laboratory Astrophysics ATTN: Prof. R. Thomas 1511 University Avenue Boulder, Colorado 80304
1	Cornell University Graduate School of Aeronautical Engineering ATTN: Prof. E. Resler Ithaca, New York 14850
1	North Carolina State University at Raleigh ATTN: Dr. Tien S. Chang 325 Riddick Laboratories Raleigh, North Carolina 27607
1	Northern Illinois University ATTN: Prof. M. Joncich DeKalb, Illinois 60115
1	Oklahoma City University Department of Physics ATTN: Prof. R. Fowler Norman, Oklahoma 73069
1	University of Pennsylvania The Towne School of Civil and Mechanical Engineering ATTN: Prof. Ira M. Cohen Philadelphia, Pa. 19104
1	University of Pennsylvania Moore School of Electrical Engineering ATTN: Prof. S. Gorn Philadelphia, Pa. 19104
1	Princeton University Palmer Physical Laboratory ATTN: Prof. W. Bleakney Princeton, New Jersey 08540
1	Princeton University Department of Aerospace and Mechanical Sciences ATTN: Prof. Wallace D. Hayes Princeton, New Jersey 08540
1	Princeton University Forrestal Research Center ATTN: Prof. S. Bogdonoff Princeton, New Jersey 08540

DISTRIBUTION LIST

No. of Copies	Organization
1	University of Southern California Engineering Center ATTN: Prof. R. Binder Los Angeles, California 90007
1	Stanford University Department of Mechanical Engineering ATTN: Prof. D. Bershader Stanfor, California 94305
1	Stevens Institute of Technology Department of Electrical Engineering ATTN: Prof. R. Geldmacher Castle Point Station Hoboken, New Jersey 07030
1	Syracuse University Department of Physics ATTN: Prof. C. Bachman Syracuse, New York 13201
1	Syracuse University Mechanical Engineering Dept ATTN: Prof. D. Dosanjh Syracuse, New York 13201
1	Temple University Department of Physics ATTN: Prof. T. Korneff Philadelphia, Pa. 19122
2	Research Institute of Temple University ATTN: Dr. A. V. Grosse Tech Lib 4150 Henry Avenue Philadelphia, Pa. 19144
1	Yeshiva University Graduate School of Mathematical Sciences ATTN: Mr. Z. Rieder Amsterdam Avenue and 186th St. New York, New York 10033

Aberdeen Proving Ground

Chief, Tech Lib
Marine Corps Ln Off
Navy Ln Off
CDC Ln Off

Unclassified
Security Classification

DOCUMENT CONTROL DATA - R & D

(Security classification of title, body of abstract and indexing annotation must be entered when the overall report is classified)

1. ORIGINATING ACTIVITY *(Corporate author)* U.S. Army Aberdeen Research and Development Center Ballistic Research Laboratories Aberdeen Proving Ground, Maryland	2a. REPORT SECURITY CLASSIFICATION Unclassified 2b. GROUP

3. REPORT TITLE

QUALITATIVE INTERFEROMETRY OF EXPANDING METAL VAPOR

4. DESCRIPTIVE NOTES *(Type of report and inclusive dates)*

5. AUTHOR(S) *(First name, middle initial, last name)*

F. D. Bennett, G. D. Kahl, and F. N. Weber, Jr.

6. REPORT DATE	7a. TOTAL NO. OF PAGES	7b. NO. OF REFS
October 1969	37	3

8a. CONTRACT OR GRANT NO.	9a. ORIGINATOR'S REPORT NUMBER(S)
b. PROJECT NO. RDT&E Project No. 1T061102A33D	Report No. 1454
c.	9b. OTHER REPORT NO(S) *(Any other numbers that may be assigned this report)*
d.	

10. DISTRIBUTION STATEMENT

This document has been approved for public release and sale; its distribution is unlimited.

11. SUPPLEMENTARY NOTES	12. SPONSORING MILITARY ACTIVITY
None	U. S. Army Materiel Command Washington, D. C.

13. ABSTRACT

The metal vapor from a wire exploded in a gas is assumed to be contained between the walls of a hollow cylinder which has boundaries that are linear functions of time. It is shown that the presence of the ambient gas can be ignored in the qualitative descriptions of the flow determined from interferograms. Studies of the single and multiple fringe interferograms expected from such a cylindrical flow are made. Graphical plotting techniques are developed to obtain these expected interferograms, and supplementary mathematical relations describing the interferograms are demonstrated. Finally, comparison of interferograms obtained by these methods is made with those interferograms obtained during actual exploding wire experiments.

DD FORM 1 NOV 65 1473 REPLACES DD FORM 1473, 1 JAN 64, WHICH IS OBSOLETE FOR ARMY USE.

Unclassified
Security Classification

Unclassified

Security Classification

14. KEY WORDS	LINK A		LINK B		LINK C	
	ROLE	WT	ROLE	WT	ROLE	WT
Time-Resolved Interferometry						
Cylindrical Blast Waves						
High Temperature Metals						
Radial Flow						
Exploding Wires						

Unclassified

Security Classification